A Data-Driven Method With Mode Decomposition Mechanism for Remaining Useful Life Prediction of Lithium-Ion Batteries

Jianguo Wang, Shude Zhang, *Student Member, IEEE*, Chenyu Li, Lifeng Wu, and Yingzhou Wang

***Abstract*—Lithium-ion batteries offer excellent advantages of high efficiency, small size, and low cost, but their instability and inconformity remain challenging. Sudden failure of batteries may cause serious accidents, endangering the safety of people's lives and properties. Advanced remaining useful life prediction methods for batteries can effectively avoid those accidents. In this article, we proposed a novel hybrid method with the purpose of enhancing battery remaining useful life prediction precision and robustness. Based on improved complete ensemble empirical mode decomposition with adaptive noise algorithm, utilizing a special-designed interpolation reconstruction mechanism, the battery capacity degradation series was decomposed into a trend subseries and several fluctuation subseries. Weighted least square support vector machine and long short-term memory network are then established to perform prediction for the trend subseries and the fluctuation ones, respectively. A complementary series of experiments is designed to verify the effectiveness of the proposed method. The simulation results represent that the proposed method achieves higher prediction accuracy and robustness over other comparison models. The proposed approach provides a promising and effective alternate for lithium-ion batteries remaining useful life prediction without relying on the cell dynamic process, which is meaningful for cases with limited measurement parameters or limited computational power.**

***Index Terms*—Empirical mode decomposition (EMD), lithium-ion battery (LIB), long short-term memory (LSTM), remaining useful life (RUL) prediction, support vector machine (SVM).**

I. Introduction

COMPARED with other energy storage forms, lithium-ion batteries (LIBs) have outstanding advantages, such as high energy density, low self-discharge rate, long lifetime, and environmental friendly [1], [2]. Therefore, LIBs have been widely used in electric vehicles and microgrid energy storage systems due to increasing concerns about fossil fuel consumption and carbon emissions worldwide [3], [4]. However, electrochemical constituents in LIBs degrades over time and use, leading to the performance deterioration, represented as capacity and power fade [5]. Generally, a capacity fade over 20% signifies end-of-life (EoL) for LIBs [6], batteries that exceed this threshold are more likely to cause malfunction, leading to serious economic losses and safety risks [7], [8]. To ensure the reliability and safety of LIBs in the case of aging, advanced remaining useful life (RUL) forecasting techniques are urgently required. However, this purpose will be difficult to achieve due to the uncertainty and complexity of the interactions inside LIBs. Over the years, various battery RUL prediction methods have been proposed to address these issues. We have seen a lot of excellent research, which can be broadly divided into two groups: model-based, and data-driven approaches.

As for the model-based approaches, electrochemical models, equivalent circuit models, empirical models, and fused models have been widely applied to simulate the cell dynamics [9], [10]. For example, Hu *et al.* [11] developed an optimization-driven moving horizon estimation framework based on a simplified electrochemical model for state of health (SOH) estimation by integrating accuracy, computational intensity, the effect of horizontal line size, and fault tolerance. Based on a second-order equivalent circuit model, Nejad *et al.* [12] applied randomly initialized a dual extended Kalman filter algorithm using pseudorandom binary sequences battery excitation to update the equivalent circuit model parameters to provide accurate estimation of battery parameters, state of charge (SOC), and state of power in real time. Based on an empirical model based on the physical degradation behavior of LIBs, He *et al.* [13] utilized Dempster–Shafer theory and Bayesian Monte Carlo method to initialize and update the model parameters, respectively. Real-time monitoring of battery capacity allows online prediction of RUL based on available data. Plett *et al.* [14] proposed a series of estimation methods for state-of-charge, power fade, capacity fade, and instantaneous available power based on extended Kalman filtering. Schwunk *et al.* [15] applied Monte Carlo sampling methods to represent the probability density function for particle filter, thereby improving the RUL prediction performance. Electrochemical modeling requires an in-depth study of the internal electrochemical reaction mechanism of the battery, such method can capture the degradation mechanism of

Manuscript received 16 April 2022; accepted 5 June 2022. Date of publication 17 June 2022; date of current version 26 July 2022. This work was partially supported in part by the Scientific and Technological Project of State Grid Corporation of China under Grant 52010119002F, and in part by the National Natural Science Foundation of China under Grant 61873175. Recommended for publication by Associate Editor S. Williamson. *(Corresponding author: Yingzhou Wang.)*

Jianguo Wang, Shude Zhang, Chenyu Li, and Yingzhou Wang are with the Jilin Province International Research Center of Precision Drive and Intelligent Control, Northeast Electric Power University, Jilin 132012, China (e-mail: ssrs8706@163.com; shudezhang@outlook.com; 19982667211@163.com; wangyingzhou@ncepu.edu.cn).

Lifeng Wu is with the College of Information Engineering, Capital Normal University, Beijing 100048, China (e-mail: wulifeng@cnu.edu.cn).

Color versions of one or more figures in this article are available at https://doi.org/10.1109/TPEL.2022.3183886.

Digital Object Identifier 10.1109/TPEL.2022.3183886

the battery well, but has too much computational overhead and is difficult to extrapolate to other types of battery cells. Equivalent circuit models or empirical models are relatively easier to build, but they are difficult to apply to the prediction of long-term evolutionary trends due to the changes of internal parameters during the use of the battery.

Utilizing advanced machine learning algorithms, data-driven approaches implement RUL prediction rely on historical aging data [16], including artificial intelligence, statistical analysis, and signal processing methods. Long *et al.* [17] used an improved autoregressive model by particle swarm optimization to predict battery capacity fade. Based on support vector regression (SVR). Wei *et al.* [18] built a battery capacity degradation model to simulate battery aging mechanism and estimate battery SOH and RUL. To reduce the computational complexity of the kernel function, Wang *et al.* [19] employed artificial bee colony and SVR to improve the prediction accuracy, and proposed a method based on improved ant lion optimization and SVR to accurately the RUL of LIBs latter [20]. Applied Box–Cox transformation and Monte Carlo simulation, Zhang *et al.* [21] proposed an RUL prediction method that needs less historical data and less time spent. Zhang *et al.* [22] applied long short-term memory (LSTM) neural networks to learn the long-term dependencies between the degraded capacities of LIBs. To address the overfitting problem of LSTM, they developed a dropout technique in a later research. Gou *et al.* [23] combined autoencoder, convolutional neural networks, and LSTM to mine deeper information in limited data. Che *et al.* [24] used Gaussian process regression (GPR) to optimize the threshold of health indicators, designed a hybrid prediction model based on transfer learning and gated recurrent neural networks to predict the RUL directly based on the optimized health indicators, in addition, applied a self-correction strategy to retrain the regression model. Chehade *et al.* [25] proposed a capacity prediction method for LIB cells based on GPR model by introducing an uncertainty measure to cross-correlate the capacity trends of different battery cells. A latent function decomposition method using multioutput convolved Gaussian process is further proposed by Chehade *et al.* [26] to capture the subtle cross-correlations between the capacity trends of available battery cells, ensuring the validity of long-term capacity prediction. The RUL prediction of LIB based on data-driven approach does not assume any explicit mathematical model to describe the aging behavior of the battery, and the prediction effect depends mainly on the quality of the historical test dataset, which is also very sensitive to the structure and parameters of the data-driven models, and most of the existing studies only train and validate the models under fixed cycling conditions, which means the robustness in practical applications has to be verified.

Although many excellent studies are conducted, data-driven techniques still have some shortcomings, requiring a large amount of aging data, and relying the quantity of measured data [27], which is usually polluted by various noises and abnormal operation. In addition, the nonlinear and nonstationary characteristics of the battery can be difficult to capture. Empirical mode decomposition (EMD) is used to analyze nonlinear and nonstationary signal by adaptively decomposing the signal into a series of zero mean oscillation modes called intrinsic mode functions (IMFs) [28]. Zhou *et al.* [29] combined autoregressive integrated moving average model with EMD to improve the prediction accuracy. Zhang *et al.* [30] used EMD to denoise the measured capacity data. Ideal prediction results are obtained by using the denoised data as the input of multiple kernel relevance vector machines. After the aging data was decomposed by EMD, Liu *et al.* [31] applied LSTM to estimate the residual component, while the GPR is utilized to fit the IMFs.

Usually, those decomposition-based hybrid models first decompose the entire dataset into several subseries iteratively, which leads to some concerns about the so-called information leakage phenomenon. Since the future data supposed to be unknown is often involved during the decomposition procedure, this decomposition-based prediction procedure is impossible to implement in the practical application. When establishing a decomposition-based time series prediction model, strict attentions needs to be taken that no future data get involved before and during the model training stage.

The main contributions of our study are made as follows.

1) A novel hybrid battery RUL prediction framework called ICEEMDAN-WLS-SVM-LSTM is developed by combing ICEEMDAN algorithm, WLS-SVM and LSTM neural network.
2) ICEEMDAN is applied to decompose the preprocessed capacity degradation series into several relatively stationary ones and a trend one in accordance with their frequency differences.
3) The decomposed data are adittionally reconstructed using an adaptive interpolation mechanism to ensure data integrity and smoothness, while avoiding information leakage situations.
4) The trend subseries are predicted by the WLS-SVM model, while the fluctuation subseries prediction is represented by the LSTM neural network.
5) The proposed data-driven approach is derived, verified, and compared to several benchmark methods on two groups of experimental LIB aging datasets. The results show the effectiveness of the proposed method.

The rest of this article is organized as follows. Section II introduces the proposed hybrid ICEEMDAN-WLS-SVM-LSTM method for RUL prediction. Section III describes the battery cycle aging data as well as the experimental protocol to validate the proposed hybrid method. Section IV validates the proposed method using battery datasets collected under different operating conditions. Finally, Section V concludes this article.

II. Method Establishment

A. Improved Complete Ensemble Empirical Model Decomposition With Adaptive Noise

Battery capacity degradation sequence usually has strong nonlinear and nonstationary characteristics, making accurate prediction difficult to achieve. EMD family algorithms are effective methods to analyze nonlinear and nonstationary signals. To eliminate the so-called mode-mixing issue existing in EMD, an ensemble version (EEMD) [32] was proposed. However, the

number of IMFs obtained by EEMD is often not equality when the signal contains some noise. Complete ensemble empirical mode decomposition with adaptive noise (CEEMDAN) [33] solves this problem by adding gaussian white noise to the original signal. In order to further eliminate the residual noise, Colominas *et al.* [34] provided an improved version called ICEEMDAN The calculation process includes the following steps.

1) Add special noise to the original signal $x(t)$, obtain the reconstructed sequence

$$x^{(i)}(t) = x(t) + \beta_0 E_1\left[w^{(i)}\right] \tag{1}$$

where $E_k[\cdot]$ denotes an EMD operator that produces the kth component after the Gaussian white noise is decomposed by EMD. $w^{(i)}$ depicts the implementation of the ith Gaussian white noise, β_0 is the magnitude of noise.

2) Apply EMD to calculate the local mean of the reconstructed sequence $x^{(i)}(t)$, take the average to obtain the first residual (RES) r_1 and the first IMF $\tilde{d}_1$

$$r_1 = \frac{1}{I}\sum_{i=1}^{I} M\left\{x^{(i)}(t)\right\} \tag{2}$$

$$\tilde{d}_1 = x(t) - r_1 \tag{3}$$

where $M\{\cdot\}$ represents the operator that calculates the local mean.

3) Calculate the second RES and IMF

$$r_2 = \frac{1}{I}\sum_{i=1}^{I} M\left\{r_1 + \beta_1 E_2\left[w^{(i)}\right]\right\} \tag{4}$$

$$\tilde{d}_2 = r_1 - r_2. \tag{5}$$

4) Repeat the abovementioned steps to calculate the value of the kth ($k = 3, 4, \ldots, N$) RES and IMF

$$r_k = \frac{1}{I}\sum_{i=1}^{I} M\left\{r_{k-1} + \beta_{k-1} E_K\left[w^{(i)}\right]\right\} \tag{6}$$

$$\tilde{d}_k = r_{k-1} - r_k. \tag{7}$$

ICEEMDAN can extract the long-term trend and short-term fluctuation of battery capacity attenuation sequence carefully, and we can take different treatments according to the different natural frequencies of each subsequence, so as to obtain accurate RUL prediction results.

It is worth noting that we introduce mirror symmetry continuation technique to reduce the effect of the end effect caused by partial decomposition by ICEEMDAN. Taking the boundary of both ends of the signal as symmetry, the signal is mapped outward to obtain the mirror image of the original signal, forming a closed curve, thus obtaining the complete envelope curve.

B. Weighted Least Squares Support Vector Machine (SVM)

Developed from statistical learning theory, SVM [35] is a powerful model having been used to solve limited sample learning problems, and has certain advantages for statistical analysis of small samples and nonlinearities. Considering equality constraints, utilizing least squares cost function, Suykens *et al.* [36] proposed least squares SVM (LS-SVM) to simplify structure and improve learning speed, further proposed a weighted version of LS-SVM (WLS-SVM) to suppress noise and obtain robust estimates for regression.

Given a training set $\{x_k, d_k\}_{k=1}^{l}$ with l samples, where $x_k \in \mathbf{R}^p$ is the input data, $(d_k = y_k + \xi_k) \in \mathbf{R}$, y_k is the output data, and ξ_k is random noise. In primal weight space, solve the optimization problem as follow according to the principle of minimizing structural risk:

$$\begin{aligned} \min_{\omega,b,\xi} J(\omega,\xi) &= \frac{1}{2}\omega^{\mathrm{T}}\omega + \frac{1}{2}\gamma\sum_{k=1}^{l} v_k\xi_k^2 \\ \text{s.t.} \quad d_k &= \omega^{\mathrm{T}}\varphi(x_k) + b + \xi_k, \quad k = 1, \ldots, l. \end{aligned} \tag{8}$$

Computing the function in dual space. Define the Lagrangian

$$\begin{aligned} \mathscr{L}(\omega, b, \xi; \alpha) &= J(\omega,\xi) \\ &\quad - \sum_{i=1}^{l}\alpha_k\left\{\omega^{\mathrm{T}}\varphi(x_k) + b + \xi_k - d_k\right\}. \end{aligned} \tag{9}$$

The Karush–Kuhn–Tucker (KKT) conditions for optimality are given by

$$\begin{cases} \dfrac{\partial\mathscr{L}}{\partial\omega} = 0 \to \omega = \sum\limits_{k=1}^{l}\alpha_k\varphi(x_k) \\ \dfrac{\partial\mathscr{L}}{\partial b} = 0 \to \sum\limits_{k=1}^{l}\alpha_k = 0 \\ \dfrac{\partial\mathscr{L}}{\partial e_k} = 0 \to \alpha_k = \gamma e_k \\ \dfrac{\partial\mathscr{L}}{\partial\alpha_k} = 0 \to \omega^T\varphi(x_k) + b + \xi_k - d_k = 0. \end{cases} \tag{10}$$

Consider the optimality conditions and elimate ω, ξ, we get the KKT system

$$\left[\begin{array}{c|c} 0 & 1_v^{\mathrm{T}} \\ \hline 1_v & \Omega + V_\gamma \end{array}\right]\left[\begin{array}{c} b \\ \hline \alpha \end{array}\right] = \left[\begin{array}{c} 0 \\ \hline d \end{array}\right] \tag{11}$$

where $d = [d_1, \ldots, d_l]$, $1_v = [1, \ldots, 1]$, $\alpha = [\alpha_1, \ldots, \alpha_l]$, and $\Omega = K(x, x_k)$ are the kernel matrices. $K(x_i, x_j)$ is a kernel function that satisfies finitely positive semidefinite, we focus on the radial basis function (RBF) kernel function

$$K(x_i, x_j) = \exp\left\{-\frac{\|x_i - x_j\|_2^2}{2\sigma^2}\right\} \tag{12}$$

where σ indicates the radius of the RBF function, which is crucial for prediction accuracy. The diagonal matrix V_γ can be given by

$$V_\gamma = \operatorname{diag}\left\{\frac{1}{\gamma v_1}, \ldots, \frac{1}{\gamma v_l}\right\}. \tag{13}$$

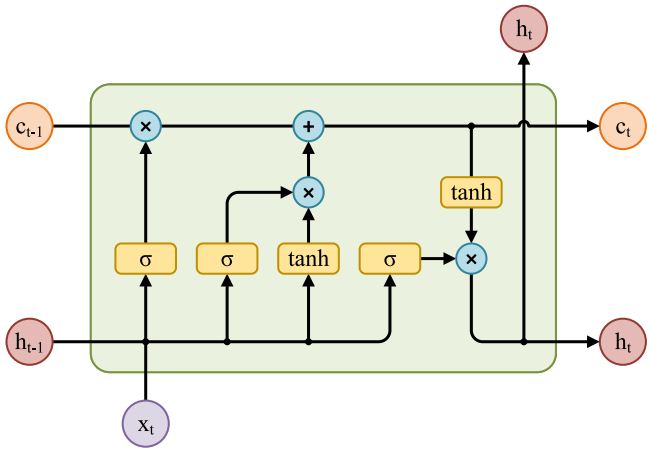

Fig. 1. Architectural of LSTM network containing three gates.

The weight factors v_k can be resolved by taking the error variables ξ_k

$$v_k = \begin{cases} 1 & \text{if } |\xi_k/\hat{s}| \leqslant c_1 \\ \dfrac{c_2 - |\xi_k/\hat{s}|}{c_2 - c_1} & \text{if } c_1 \leqslant |\xi_k/\hat{s}| \leqslant c_2 \\ 10^{-4} & \text{else} \end{cases} \tag{14}$$

$\hat{s}$ provides a robust estimation of the standard deviation

$$\hat{s} = \frac{\text{IQR}}{2 \times 0.6745}. \tag{15}$$

IRQ indicates the distance between the upper quartile and lower quartile of ξ_k. According to Rousseeuw [37], the constants c_1, c_2 are usually chosen as 2.5 and 3, respectively. Thus, the regression function of WLS-SVM can be represented by

$$\hat{d}(x) = \sum_{i=1}^{l} \alpha_k K(x, x_k) + \text{b}. \tag{16}$$

Usually, WLS-SVM uses quadratic loss function, which turns all training samples into the so-called support vectors, thus has the ability to perceive all training samples. Therefore, the battery RUL prediction model established based on WLS-SVM is expected to obtain good robustness prediction results when dealing with challenges of various working conditions or abnormal data samples.

C. Long Short-Term Memory

First proposed in 1997, LSTM neural network [38] adds cell state and gate structure on the basis of traditional RNN. Each LSTM neuron contains one memory cell and three control gates. The memory cell stores information, which will be updated by input gate, forget gate, and output gate. Take advantage of this structure, LSTM have the ability to establish a long-term dependency between input and feedback. The continuous information flow is stored in the memory unit, thus solving the problems of gradient disappearance and gradient explosion that exist in traditional RNNs. The structure of a single LSTM unit is shown in Fig. 1.

The forgetting gate decides to retain or forget the output h_{t-1} at the previous moment, and uses sigmoid function to generate a weight between 0 (complete forgetting) and 1 (complete retention)

$$f_t = \sigma\left(W_f \cdot [h_{t-1}, x_t] + b_f\right) \tag{17}$$

where W_f is the weight matrix of forget gate, and b_f is the bias, σ denotes the sigmoid function

$$\sigma(x) = \frac{1}{1 + \text{e}^{-x}}. \tag{18}$$

The input gate is used to update the cell state and determines the weight in which new information is incorporated into the cell state. The sigmoid function in the input gate generates a weight between 0 and 1

$$i_t = \sigma\left(W_i \cdot [h_{t-1}, x_t] + b_i\right) \tag{19}$$

where W_i and b_i are the weight matrix and the bias of the input gate, respectively. Then the value of the candidate memory cell $\widetilde{C}_t$ can be acquired

$$\widetilde{C}_t = \tanh\left(W_c \cdot [h_{t-1}, x_t] + b_c\right) \tag{20}$$

where W_c indicates the weight matrix of tanh activation function layer, and b_c is the bias.

The cell state C_t can be updated by using the output of forgetting gate and input gate

$$C_t = f_t * C_{t-1} + i_t * \widetilde{C}_t \tag{21}$$

where C_{t-1} represents the state value of the last LSTM unit. Finally, an output gate and a tanh function layer were used to generate the cell network output h_t

$$o_t = \sigma\left(W_o \cdot [h_{t-1}, x_t] + b_o\right) \tag{22}$$

$$h_t = o_t * \tanh\left(C_t\right) \tag{23}$$

where W_o is the weight matrix, and b_o is the bias.

Based on the unique control gate structure and memory cell, LSTM can better learn and remember long-term information, thus have the ability to capture the long-term capacity degradation characteristics of the LIBs effectively.

D. Proposed Model

Combining the advantages of each component, a novel hybrid LIB RUL prediction method, namely ICEEMDAN-WLS-SVM-LSTM (hereafter referred to as DE-WLSSVM-LSTM), is proposed.

Based on WLS-SVM and LSTM as basic models, ICEEMDAN is introduced to extract the long-term trend and short-term fluctuation characteristics of battery capacity degradation process, so as to achieve better prediction accuracy. The framework of the proposed hybrid DE-WLSSVM-LSTM method is illustrated in Fig. 2. This procedure includes the following detailed steps.

1) After preprocessing of raw dataset, such as culling and statistical analysis, it is divided into a training set and a test set, respectively. Future data are completely unknown

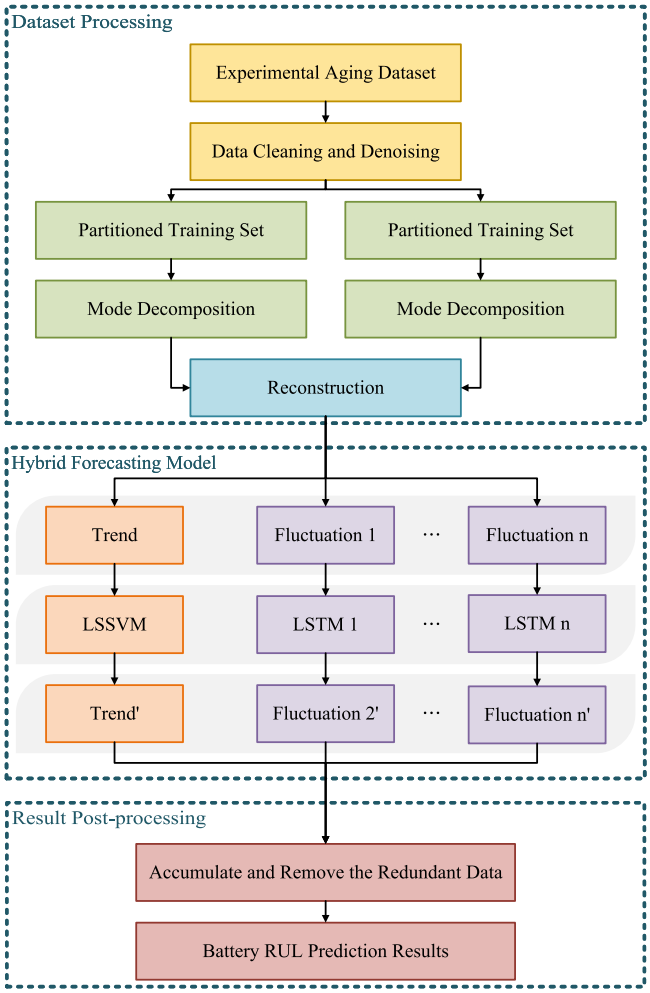

Fig. 2. Flow chart of the proposed hybrid method.

for the proposed hybrid forecasting framework, so information leakage phenomenon can be avoided.

2) ICEEMDAN is applied to excavate the traits of the training set carefully, decompose the training set into a low-frequency trend subseries, and several high-frequency fluctuation subseries.
3) Reconstruction of the decomposed training and test sets using cubic spline interpolation to fit the neural network and achieve better prediction results.
4) The trend subseries is predicted by WLS-SVM model, while the prediction of fluctuation subseries is performed by LSTM neural network.
5) The predictions obtained from each subseries are accumulated and the redundant data inserted in step 3) are removed to reconstruct the final RUL predictions.

III. Materials and Experiments

A. Data Description

The battery capacity degradation data were collected from the Center for Advanced Life Cycle Engineering (CALCE) at the University of Maryland [13], including several CS2-type batteries with a nominal capacity of 1.1Ah made of $LiCoO_2$ cathode material. The specification of the batteries is listed in Table I. All four batteries were charged under a constant current–constant voltage (CC-CV) charging protocol independently. First charged at a fixed current rate of 0.5 C until the voltage equals 4.2 V, these cells were then sustained at a constant voltage of 4.2 V until the current drops below 50 mA. Next the discharge procedure was carried out, CS2-33 and CS2-34 were discharged with a constant current rate of 0.5 C until the voltage decreases to 2.7 V, while cells marked as CS2-36 and CS2-37 were discharged under 1 C. The cyclic aging test on cell CS2-34 ended prematurely, science we mainly focused on the aging state of the battery before and near EoL, we uniformly collect only the data before their discharge capacity decayed to 0.55Ah, at which point they had cycled 715, 764, 795, and 883 times, respectively. The EoL was set to 0.77 Ah (exactly 70% of the rated capacity) in our study. The capacity attenuation tendency of the batteries with the increase of cycle numbers is shown in Fig. 3(a).

TABLE I
Specification of the Tested Battery Cells

Battery details	Value (Unit)
Rated capacity	1100 mAh
Cell chemistry	$LiCoO_2$ cathode and graphite anode
Weight	21.1 g
Dimensions	5.4 mm x 33.6 mm x 50.6 mm

However, in real-world usage scenarios, batteries rarely follow a fixed cyclic charge/discharge routine. To approximate the effect on battery life under real-world conditions of use, Prognostics Center of Excellence (PCoE) at National Aeronautics and Space Administration [39] selected four 18 650 LIBs, respectively, RW-09, RW-10, RW-11, and RW-12. These batteries were randomly charged and discharged at currents between –4.5 and 4.5 A, each process lasted 5 min, and after 1500 durations (approximately 5 days), a cyclic charge/discharge reference test was performed to provide a reference benchmark for battery condition health. The EoL is also set to 70% of rated capacity 2.0 Ah. The capacity degradation curve derived from intermittent cyclic charge/discharge sizing experiments is shown in Fig. 3(b).

B. Decomposition and Normalization of the Datasets

By using ICEEMDAN, we decompose each raw dataset into several IMFs and an RES. The amplitude of white noise added in ICEEMDAN is set to 0.2 times of the standard deviation [32]. In order to improve the adaptability and reduce the computational cost of the hybrid method, while ensuring that the number of sequences obtained from the decomposition of the training set and the dataset is consistent. The number of fluctuating subsequences obtained by ICEEMDAN is limited to 3.

Taking CS2-34 as an example, the discharge capacity data were first divided into training and test sets, and after decomposing them separately, there was a large gap between the end points of the training set and the front points of the test set, which

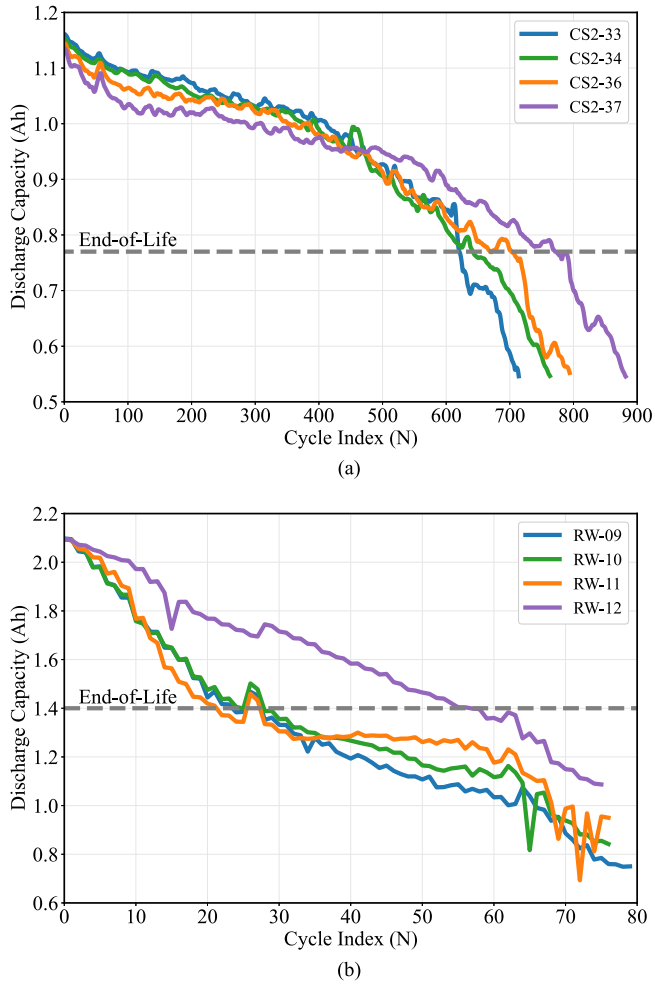

Fig. 3. Battery discharge capacity degradation curves.

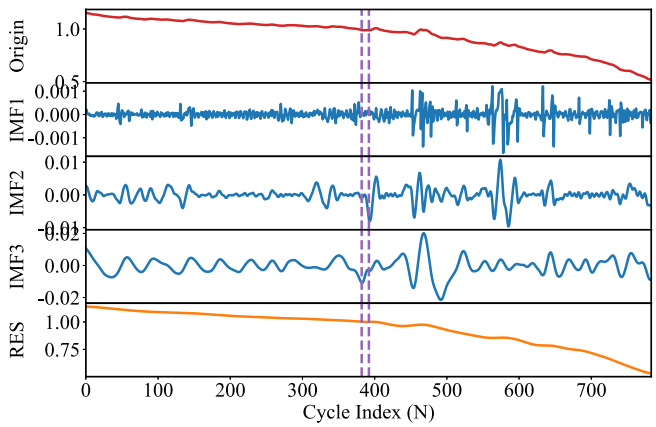

Fig. 4. Reconstructed battery discharge capacity curve after cubic spline interpolation with CS2-34 as an example.

had a negative impact on the prediction. We inserted an empty data of length 10 and used cubic spline interpolation to complete this part of the data as part of the reconstructed training set. After the prediction is completed, this part of the data is removed and the prediction results on the real training set are restored. The complete reconstructed data set is shown in Fig. 4.

Then the reconstructed subsequences is normalized and restricted to the interval $[0, 1]$ using the minimum–maximum normalization procedure

$$x(t)' = \frac{x(t) - \min x(t)}{\max x(t) - \min x(t)} \tag{24}$$

where $\min x(t)$ and $\max x(t)$ are the minimum and maximum values of the current training set, respectively. After the prediction is completed, the output can be restored by

$$x(t)_p = x(t)'_p(\max x(t) - \min x(t)) + \min x(t) \tag{25}$$

where $x(t)'_p$ is the output value of the forecasting model.

C. Experimentation Design

1) Single Forecasting Models: Before the models are trained, their hyperparameters need to be well-determined manually: (a) for WLS-SVM, its hyperparameters were optimized by a 10-fold cross validation approach; (b) for LSTM, aiming to minimize MAE on the validation set, its structure parameters, such as the number of hidden layers and their own neurons are determined according to a layer-by-layer enumeration process; (c) moreover, SVR and BP are built as comparison models based on the determined hyperparameters of WLS-SVM and LSTM, respectively.

2) Decomposition-Based Models: The well-designed experimentation flow of the decomposition-based models is illustrated in Fig. 5, and a series of decomposition-based RUL prediction models are implemented for comparison.

After the training data s being decomposed by the end-extension ICEEMDAN, the generated trend subseries s_1 and fluctuation subseries $s_2, s_3, \ldots, s_n$ are predicted by a certain single model, respectively. By summing up the forecasting result $\hat{s_1}$ of trend subseries and $\hat{s_2}, \hat{s_3}, \ldots, \hat{s_n}$ of fluctuation subseries, we get the final RUL prediction result. Consequently, four decomposition-based hybrid forecasting models are built noted as DE-WLSSVM, DE-LSTM, DE-SVR, and DE-BP.

In order to verify the validity of WLS-SVM for trend subseries and LSTM for fluctuation subseries, respectively. The following two cross-combination models can be built, namely, DE-WLSSVM-LSTM when WLS-SVM is adopted to modeling s_1 and LSTM is used to model $s_2, s_3, \ldots, s_n$, and DE-LSTM-WLSSVM otherwise.

3) Model Online Validation: To verify the model validity of the proposed hybrid DE-WLSSVM-LSTM method in practical industrial application, a forecasting procedure that is fully compliant with online situation is designed. The well-trained models are utilized for RUL prediction on cells CS2-34, CS2-37, RW-11, and RW-12, and updated with a window of 25% measured battery capacity degradation time series before the EoL.

D. Evaluation Criterion

To evaluate the prediction performance of the proposed hybrid method, three evaluation criteria are employed: mean absolute

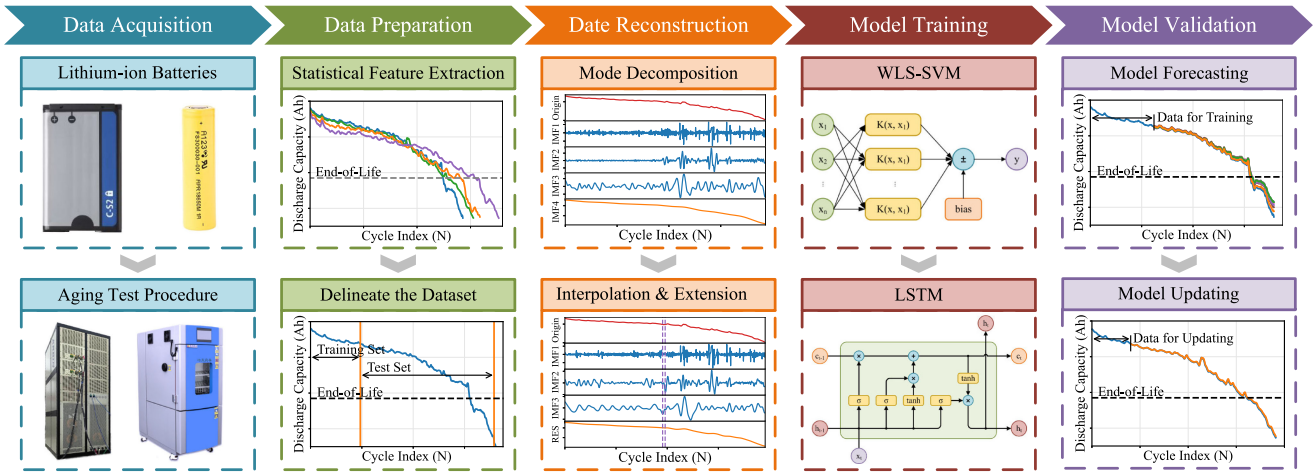

Fig. 5. Experimentation design of the decomposition-based models.

error (MAE), mean absolute percentage error (MAPE), and root-mean-square-error (RMSE)

$$\mathrm{MAE} = \frac{1}{N}\sum_{k=1}^{N}|Y(k) - \hat{Y}(k)| \tag{26}$$

$$\mathrm{MAPE} = \frac{1}{N}\sum_{k=1}^{N}\left|\frac{Y(k) - \hat{Y}(k)}{Y(k)}\right| \times 100\% \tag{27}$$

$$\mathrm{RMSE} = \sqrt{\frac{1}{N}\sum_{k=1}^{N}|Y(k) - \hat{Y}(k)|^2} \tag{28}$$

where $Y(k)$ and $\hat{Y}(k)$ denote the kth measurement capacity series and predicted capacity series, respectively. N is the number of cycles between the starting point of prediction and the actual battery EoL.

The accuracy of battery RUL prediction can be presented by the difference between the numbers of actual and predicted cycles when the capacity reaches the failure threshold. We further introduced E_r and PE_r to describe this error

$$E_r = \widehat{\mathrm{RUL}} - \mathrm{RUL} \tag{29}$$

$$PE_r = \frac{|\widehat{\mathrm{RUL}} - \mathrm{RUL}|}{\mathrm{RUL}} \times 100\% \tag{30}$$

where $\widehat{\mathrm{RUL}}$ denotes the predicted RUL value and RUL is the actual one.

IV. Results and Discussions

A. Performance Comparison of Different Models

To compare the RUL prediction performance of single models, data collected from CS2-33 is utilized to perform prediction. Its measured capacity drops below EoL at the 715th cycle, only the data from the first 248 cycles (exactly 40% before its EoL) is used as training set in this procedure.

For WLS-SVM model, we choose RBF kernal function to improve its generalization ability. The LSTM model has two hidden layers, including 100 and 50 neurons, respectively, according to the enumeration method layer-by-layer. The prediction results are shown in Table II, it is obvious that:

TABLE II
Prediction Accuracy of Single Models on CS2-33 Under 0.5 C Discharging Rate

Method	MAE	MAPE	RMSE	$\widehat{\mathrm{RUL}}$	Er
BP	0.1308	4.0837	0.0703	641	20
SVR	0.0916	3.2536	0.0523	634	13
LSTM	0.0184	2.5103	0.0271	**627**	**6**
WLSSVM	**0.0154**	**2.0839**	**0.0226**	630	9

1) WLS-SVM achieves the most precise RUL prediction result, minimum MAE, MAPE, and RMSE, while LSTM has get pretty good RUL forecasting accuracy;
2) WLS-SVM achieves the reductions of 0.6441% for PEr and 0.0477 Ah for RMSE over that of SVR, respectively;
3) LSTM decreases PEr and RMSE by 2.2544% and 0.0432 Ah in comparison with BP, respectively;
4) BP has got the worse prediction perfomance in comparison with other single models.

According to the aforementioned analysis, we come to the conclusion that WLS-SVM and LSTM each have their advantages when speaking of different evaluation metrics.

The forecasting results of the decomposition-based hybrid models with CS2-33 and CS2-36 are illustrated in Tables III and IV, respectively. The datasets are organized according to the same principles as single models. Further, two cross-combination models are established to compare the forecasting perfomance of single models with different kind of subseries, the prediction results have been attached to the tables. Due to the poorer performance of SVR and BP in abovementioned prediction experiments of single models, we are not going to consider utilizing them for cross-combination modeling. A positive Er denotes that the predicted RUL is latter than it actually is, otherwise denotes the predicted capacity drops below the EoL threshold ahead of reality. As with the single models, the starting point for prediction is the 250th cycle.

TABLE III
PREDICTION ACCURACY OF THE DECOMPOSITION-BASED MODELS FOR CS2-33 UNDER 0.5 C DISCHARGING RATE

Method	MAE(Ah)	MAPE(%)	RMSE(Ah)	RUL	$\widehat{\text{RUL}}$	Er(Cycles)	PEr(%)
LSTM	0.0184	2.5103	0.0271	621	627	6	0.9661
WLSSVM	0.0154	2.0839	0.0226	621	630	9	1.4493
DE-LSTM	0.0151	1.9433	0.0187	621	626	5	0.8051
DE-WLSSVM	0.0127	1.7453	0.0196	621	627	6	0.9661
DE-LSTM-WLSSVM	0.0153	2.1385	0.0246	621	627	6	0.9661
DE-WLSSVM-LSTM	**0.0056**	**0.7557**	**0.0082**	**621**	**624**	**3**	**0.4831**

TABLE IV
PREDICTION ACCURACY OF THE DECOMPOSITION-BASED MODELS FOR CS2-36 UNDER 1 C DISCHARGING

Method	MAE(Ah)	MAPE(%)	RMSE(Ah)	RUL	$\widehat{\text{RUL}}$	Er(Cycles)	PEr(%)
LSTM	0.0277	3.7008	0.0334	704	723	19	2.6989
WLSSVM	0.0228	3.1206	0.0301	704	719	15	2.1306
DE-LSTM	0.0224	3.0701	0.0293	704	722	18	2.5568
DE-WLSSVM	0.0214	2.9029	0.0271	704	721	17	2.4147
DE-LSTM-WLSSVM	0.0206	2.8568	0.0278	704	722	18	2.5568
DE-WLSSVM-LSTM	**0.0059**	**0.7999**	**0.0085**	**704**	**714**	**10**	**1.4205**

The RUL prediction results for cell CS2-33 by using several different decomposition-based models and the novel cross-combination are presented in Fig. 6(a). The predicted capacity of LSTM falls below the EoL threshold at the 627th cycle, with a deviation of 6 cycles (0.9661%) from the actual RUL value. For the WLSSVM model,, the predicted data present a relatively smooth trend, some details of capacity recovery are missing. The predicted RUL result reaches the 630th cycle, resulting in a 9 error cycles (1.4493%). From the results of the DE-LSTM model, and the battery is predicted to reach its EoL threshold at the 626th cycle, indicating a prediction error of 5 cycles (0.8051%). The prediction accuracy of DE-WLSSVM is better than that of DE-LSTM, resulting in a prediction error of 6 cycles (0.9661%). For the proposed hybrid DE-WLSSVM-LSTM method, its prediction result well-fitted the actual capacity degradation curves of CS2-33, produced an RUL prediction error of only 3 cycle (0.4831%) in comparison with the actual test data, which can be attributed to the fact that WLS-SVM can better fit the overall trend. Obviously, MAE, MAPE, an RMSE also achieved a significant decrease compared to other methods. As a comparison, the prediction error of DE-LSTM-WLSSVM is not significantly reduced compared to before the combination. Evidently, the proposed method can learn the degradation characteristics of batteries more effectively and performs superior to the comparative models.

Fig. 6(b) depicts the RUL prediction results for CS2-36 with a discharging rate of 1 C based on the six different models. The measured capacity of CS2-36 drops below EoL at the 704th cycle. The RUL of CS2-36 is predicted to be 723 by LSTM model, the Er and PEr still far from satisfaction, which are 19 cycles and 2.6989%, respectively. The same WLSSVM model is applied to predict the RUL of CS2-36, resulting in an error of 15 cycles (2.1306%), the MAE and RMSE are calculated as 0.0154 and 0.0226 Ah, respectively. For DE-LSTM, the predicted RUL is 644, indicating an error of 18 cycles (2.5568%), while the MAE and RMSE are 0.0224 and 0.0293 Ah, respectively, which is as unremarkable as that of CS2-33. Compared with the abovementioned common models, the proposed hybrid model achieves a 10 cycle prediction deviation compared with the measured values, indicating a comparative accuracy RUL prediction for CS2-36. This finding provides further evidence that the newly designed hybrid model is particularly efficacious for battery RUL forecasting. In order to further explore the feasibility of the proposed method in practical applications, randomly charged and discharged RW9 and RW10 with 40% of the data before EoL were used as the training set to perform the RUL prediction task. Fig. 7(a) depicts the RUL prediction results for RW-09. The measured capacity of RW-09 drops below EoL at the 25th cycle. The models with a mixture of WLSSVM has better forecasting results for tracking the overall trend, however loses detailed information on local volatility.

We can see that the prediction performance of most data-driven methods deteriorates dramatically due to the large reduction of available data in the training set of the random walk datasets, while our proposed method still provides reliable RUL prediction results. The corresponding Ers for RW-09 and RW-10 are 3, and 1, respectively, according to Table VI. This finding suggests that the presented method is more likely to achieve robust RUL predictions with less available data than other data-driven methods.

B. Model Online Validation

To verify the model validity for online forecasting of the proposed hybrid forecasting method, two cells with the same specification, namely CS2-34 and CS2-37, respectively, dischargrd at 0.5 C and 1 C, are utilized for testing. The well-trained models are designed to be continually updated with a slide window that contains 25% measured battery capacity data before the EoL, then the RUL prediction tasks are executed. The quantitative

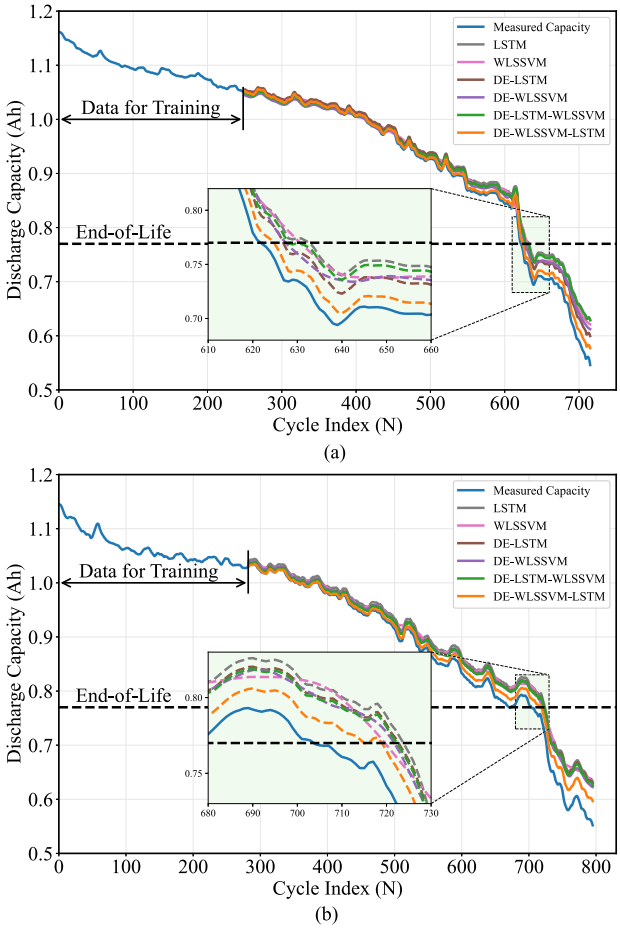

Fig. 6. Diagrams of prediction results for cyclic used LIB degradation data.

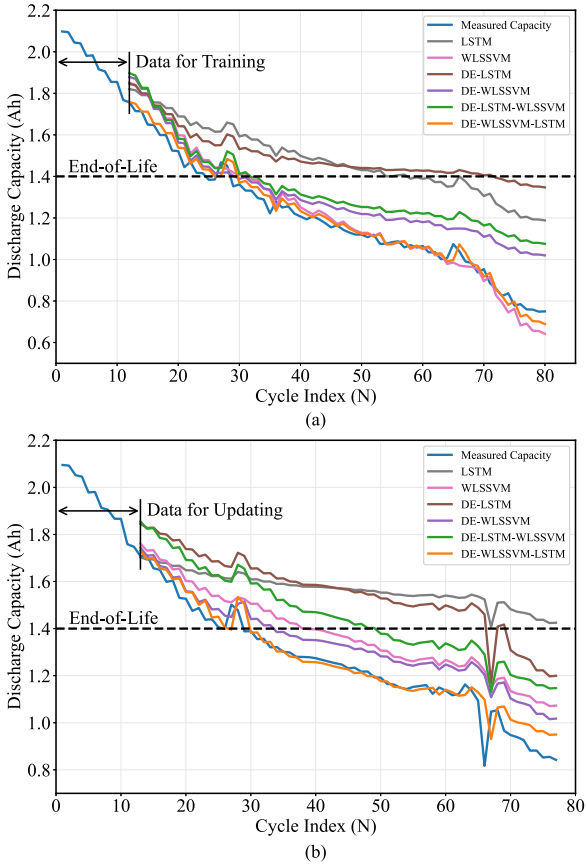

Fig. 7. Diagrams of prediction results for random walk LIB degradation data.

TABLE V
PREDICTION PERFORMANCE FOR CALCE FIXED CYCLIC CHARGING AND DISCHARGING DATASETS BASED ON THE PROPOSED METHOD

	CS2-33	CS2-34	CS2-36	CS2-37
EoL (Ah)	0.77	0.77	0.77	0.77
STL/UDL*	250	162*	283	195*
RUL	621	642	704	772
$\widehat{\text{RUL}}$	624	645	714	777
Er (Cycles)	3	3	10	5
PEr (%)	0.4821	0.4666	1.4205	0.6477
MAE (Ah)	0.0056	0.0037	0.0059	0.0037
MAPE (%)	0.7557	0.4715	0.7999	0.4509
RMSE (Ah)	0.0082	0.0047	0.0085	0.0042

results of the RUL prediction for the selected four batteries using the proposed model are listed in Table V, in which STL indicates the prediction start line for well-trained model, and UDL* denotes the prediction start point for updated model.

The battery RUL prediction results for battery CS2-34 with the previously trained models are illustrated in Fig. 8(a). The failure threshold was reached on the 642th cycle. Adapting a rolling forward strategy to update the proposed DE-WLSSVM-LSTM RUL forecasting model, the sliding window size is set to 162 cycles (actually 25% before EoL). The predicted result reaches EoL at the 645th cycle, indicating 3 cycles (0.4666%) earlier than the real RUL. The calculated MAPE and RMSE are 0.4715% and 0.0047 Ah, respectively. This finding proves that the proposed model can be realized for online RUL prediction without the need to repeat the whole training process. With a close observation of the curves, the capacity prediction exhibits a meticulous transformation than sate-of-the-art models.

For cell CS2-37, the RUL prediction results are described in Fig. 8(b). The battery reaches EoL at the 772th cycle under 1 C discharging rate. The well-trained models are updated with decomposed offline data of the first 195 cycles (actually 25% before EoL). The test results indicate that the proposed method produces a 5-cycles-longer (0.6477%) error compared with the real RUL, and the MAE and RMSE of the whole forecasting process are as low as 0.0037 and 0.0042 Ah, respectively. Obviously, the proposed hybrid DE-WLSSVM-LSTM model has excellent capability in terms of RUL prediction accuracy, consistency, and robustness of the aging process over other methods.

The battery RUL prediction results for battery RW-11 with the previously trained models are illustrated in Fig. 9(a). Very little data are available to update the well-trained forecasting model, only capacity data from the first nine standard charge/discharge experiments. Nevertheless, the proposed hybrid DE-WLSSVM-LSTM model achieves incredible prediction results. The predicted result reaches EoL at the 29th cycle, indicating only 1 cycle (3.5714%) latter than the real RUL. The calculated MAPE and RMSE are 3.9473% and 0.0715 Ah, respectively. The same

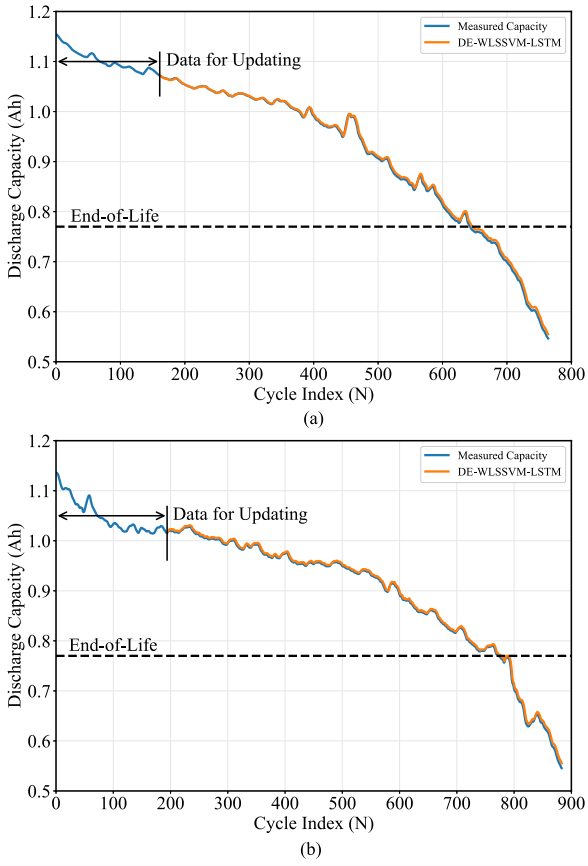

Fig. 8. Prediction results for CS2-34 and CS2-37 using the proposed method with a small amount of data to update the model.

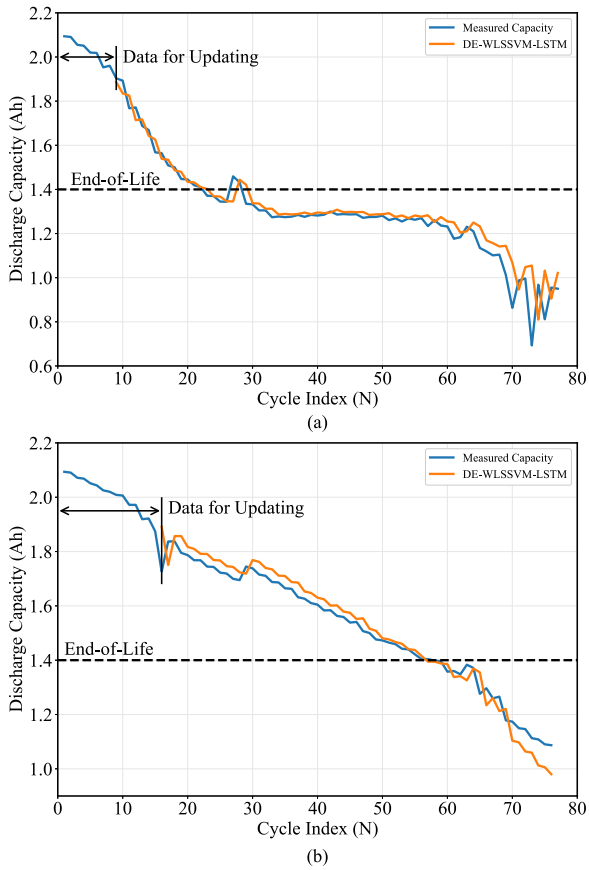

Fig. 9. Prediction results for RW-11 and RW-12 using the proposed method with a small amount of data to update the model.

TABLE VI
PREDICTION PERFORMANCE FOR PCOE RANDOM WALK BATTERY CHARGING AND DISCHARGING DATASETS BASED ON OUR METHOD

	RW-09	RW-10	RW-11	RW-12
EoL (Ah)	1.4	1.4	1.4	1.4
STL/UDL*	12	13	9*	16*
RUL	25	29	28	59
$\widehat{\text{RUL}}$	28	30	29	58
Er (Cycles)	3	1	1	-1
PEr (%)	12	3.4483	3.5714	1.6949
MAE (Ah)	0.0313	0.0366	0.0415	0.0380
MAPE (%)	2.7540	3.4045	3.9473	2.6463
RMSE (Ah)	0.0402	0.0588	0.0715	0.0480

phenomenon is also seen in the predicted results for RW-12 in Fig. 9(b), for which the proposed method accurately captures the aging path, despite that the discharge capacity decay curve of RW-12 shows a much slower decreasing trend. The proposed method produces a 1 cycle ahead (1.6949%) error compared with the real RUL, and the MAE and RMSE of the whole forecasting process are as low as 0.0380 and 0.0480 Ah, respectively.

V. CONCLUSION

A novel hybrid RUL prediction method for LIBs based on ICEEMDAN, WLS-SVM, and LSTM algorithms is proposed in this study. The hybrid method has the advantages of dealing with nonstationary, nonlinear time series compared with other popular intelligent algorithms.

The proposed hybrid model can achieve accurate RUL prediction of LIBs on the basis of ICEEMDAN, WLS-SVM, and LSTM model. The key factors include dealing with the nonstationary, nonlinear capacity degradation data series and preventing LSTN from overfitting. A multiple improved EMD family algorithm was used to decompose the dataset into some stationary ones in accordance with their frequency characteristics. The specialized dropout technique with minibatch method were applied to improve the regression performance of LSTM-RNN. Further, by first dividing the dataset into a training set and a test set, and then performing an adaptive interpolation mechanism, the test set cannot obtain *a priori* knowledge from the training set, thus the information leakage phenomenon usually caused by using decomposition-based prediction methods is addressed.

Utilized two groups of degraded datasets with a total of eight batteries for discharge capacity, the applicability of the proposed method under fixed-cycle and random-walk conditions was fine verified, respectively. The prediction results of other methods are compared with those of the proposed method to verify the efficacy of the latter. The results show that the RUL prognosis of our hybrid method is accurate and stable. Specifically, the RMSE of the proposed hybrid ICEEMDAN-WLS-SVM-LSTM

method is less than 0.05, and the PEr value for most cells is less than 4%. The cross-comparison results indicate that the proposed hybrid method can predict the RUL of LIBs effectively. The online validation results indicate the ideal generalization ability of the hybrid method.

REFERENCES

[1] G. Dong, X. Zhang, C. Zhang, and Z. Chen, "A method for state of energy estimation of lithium-ion batteries based on neural network model," *Energy*, vol. 90, pp. 879–888, Oct. 2015.

[2] Y. Xiao, "Model-based virtual thermal sensors for lithium-ion battery in EV applications," *IEEE Trans. Ind. Electron.*, vol. 62, no. 5, pp. 3112–3122, May 2015.

[3] X. Hu, C. Zou, C. Zhang, and Y. Li, "Technological developments in batteries: A survey of principal roles, types, and management needs," *IEEE Power Energy Mag.*, vol. 15, no. 5, pp. 20–31, Sep./Oct. 2017.

[4] J. Wang, S. Lu, Y. Wang, C. Li, and K. Wang, "Effect analysis on thermal behavior enhancement of lithium–ion battery pack with different cooling structures," *J. Energy Storage*, vol. 32, Dec. 2020, Art. no. 101800.

[5] L. Zhang, X. Hu, Z. Wang, F. Sun, J. Deng, and D. G. Dorrell, "Multiobjective optimal sizing of hybrid energy storage system for electric vehicles," *IEEE Trans. Veh. Technol.*, vol. 67, no. 2, pp. 1027–1035, Feb. 2018.

[6] P. L. T. Duong and N. Raghavan, "Heuristic Kalman optimized particle filter for remaining useful life prediction of lithium-ion battery," *Microelectron. Rel.*, vol. 81, pp. 232–243, Feb. 2018.

[7] R. R. Richardson, M. A. Osborne, and D. A. Howey, "Gaussian process regression for forecasting battery state of health," *J. Power Sources*, vol. 357, pp. 209–219, Jul. 2017.

[8] X. Li, Z. Wang, L. Zhang, C. Zou, and D. D. Dorrell, "State-of-health estimation for Li-ion batteries by combing the incremental capacity analysis method with grey relational analysis," *J. Power Sources*, vol. 410–411, pp. 106–114, Jan. 2019.

[9] G. L. Plett, *Battery Management Systems: Battery Modeling*, vol. 1. Norwood, MA, USA: Artech House, 2015.

[10] X. Hu, L. Xu, X. Lin, and M. Pecht, "Battery lifetime prognostics," *Joule*, vol. 4, no. 2, pp. 310–346, Feb. 2020.

[11] X. Hu, D. Cao, and B. Egardt, "Condition monitoring in advanced battery management systems: Moving horizon estimation using a reduced electrochemical model," *IEEE/ASME Trans. Mechatron.*, vol. 23, no. 1, pp. 167–178, Feb. 2018.

[12] S. Nejad and D. T. Gladwin, "Online battery state of power prediction using PRBS and extended Kalman filter," *IEEE Trans. Ind. Electron.*, vol. 67, no. 5, pp. 3747–3755, May 2020.

[13] W. He, N. Williard, M. Osterman, and M. Pecht, "Prognostics of lithium-ion batteries based on Dempster-Shafer theory and the Bayesian Monte Carlo method," *J. Power Sources*, vol. 196, no. 23, pp. 10314–10321, 2011.

[14] G. L. Plett, "Extended Kalman filtering for battery management systems of LiPB-based HEV battery packs," *J. Power Sources*, vol. 134, no. 2, pp. 277–292, Aug. 2004.

[15] S. Schwunk, N. Armbruster, S. Straub, J. Kehl, and M. Vetter, "Particle filter for state of charge and state of health estimation for lithium–iron phosphate batteries," *J. Power Sources*, vol. 239, pp. 705–710, Oct. 2013.

[16] X. Hu, J. Jiang, D. Cao, and B. Egardt, "Battery health prognosis for electric vehicles using sample entropy and sparse Bayesian predictive modeling," *IEEE Trans. Ind. Electron.*, vol. 63, no. 4, pp. 2645–2656, Apr. 2016.

[17] B. Long, W. Xian, L. Jiang, and Z. Liu, "An improved autoregressive model by particle swarm optimization for prognostics of lithium-ion batteries," *Microelectron. Rel.*, vol. 53, no. 6, pp. 821–831, Jun. 2013.

[18] J. Wei, G. Dong, and Z. Chen, "Remaining useful life prediction and state of health diagnosis for lithium-ion batteries using particle filter and support vector regression," *IEEE Trans. Ind. Electron.*, vol. 65, no. 7, pp. 5634–5643, Jul. 2018.

[19] Y. Wang, Y. Ni, S. Lu, J. Wang, and X. Zhang, "Remaining useful life prediction of lithium-ion batteries using support vector regression optimized by artificial bee colony," *IEEE Trans. Veh. Technol.*, vol. 68, no. 10, pp. 9543–9553, Oct. 2019.

[20] Y. Wang *et al.*, "A method based on improved ant lion optimization and support vector regression for remaining useful life estimation of lithium-ion batteries," *Energy Sci. Eng.*, vol. 7, no. 6, pp. 2797–2813, Dec. 2019.

[21] Y. Zhang, R. Xiong, H. He, and M. G. Pecht, "Lithium-ion battery remaining useful life prediction with Box–Cox transformation and Monte Carlo simulation," *IEEE Trans. Ind. Electron.*, vol. 66, no. 2, pp. 1585–1597, Feb. 2019.

[22] Y. Zhang, R. Xiong, H. He, and M. G. Pecht, "Long short-term memory recurrent neural network for remaining useful life prediction of lithium-ion batteries," *IEEE Trans. Veh. Technol.*, vol. 67, no. 7, pp. 5695–5705, Jul. 2018.

[23] B. Gou, Y. Xu, and X. Feng, "State-of-health estimation and remaining-useful-life prediction for lithium-ion battery using a hybrid data-driven method," *IEEE Trans. Veh. Technol.*, vol. 69, no. 10, pp. 10854–10867, Oct. 2020.

[24] Y. Che, Z. Deng, X. Lin, L. Hu, and X. Hu, "Learning and online model correction," *IEEE Trans. Veh. Technol.*, vol. 70, no. 2, pp. 1269–1277, Feb. 2021.

[25] A. A. Chehade and A. A. Hussein, "A collaborative Gaussian process regression model for transfer learning of capacity trends between li-ion battery cells," *IEEE Trans. Veh. Technol.*, vol. 69, no. 9, pp. 9542–9552, Sep. 2020.

[26] A. A. Chehade and A. A. Hussein, "A multioutput convolved Gaussian process for capacity forecasting of li-ion battery cells," *IEEE Trans. Power Electron.*, vol. 37, no. 1, pp. 896–909, Jan. 2022.

[27] Y. Li *et al.*, "Data-driven health estimation and lifetime prediction of lithium-ion batteries: A review," *Renew. Sustain. Energy Rev.*, vol. 113, Oct. 2019, Art. no. 109254.

[28] N. E. Huang *et al.*, "The empirical mode decomposition and the Hilbert spectrum for nonlinear and non-stationary time series analysis," *Proc. Roy. Soc. London Ser. Math. Phys. Eng. Sci.*, vol. 454, no. 1971, pp. 903–995, Mar. 1998.

[29] Y. Zhou and M. Huang, "Lithium-ion batteries remaining useful life prediction based on a mixture of empirical mode decomposition and ARIMA model," *Microelectron. Rel.*, vol. 65, pp. 265–273, Oct. 2016.

[30] C. Zhang, Y. He, L. Yuan, and S. Xiang, "Capacity prognostics of lithium-ion batteries using EMD denoising and multiple kernel RVM," *IEEE Access*, vol. 5, pp. 12061–12070, 2017.

[31] K. Liu, Y. Shang, Q. Ouyang, and W. D. Widanage, "A data-driven approach with uncertainty quantification for predicting future capacities and remaining useful life of lithium-ion battery," *IEEE Trans. Ind. Electron.*, vol. 68, no. 4, pp. 3170–3180, Apr. 2021.

[32] Z. Wu and N. E. Huang, "Ensemble empirical mode decomposition: A noise-assisted data analysis method," *Adv. Adaptive Data Anal.*, vol. 01, no. 01, pp. 1–41, Jan. 2009.

[33] M. E. Torres, M. A. Colominas, G. Schlotthauer, and P. Flandrin, "A complete ensemble empirical mode decomposition with adaptive noise," in *Proc. IEEE Int. Conf. Acoust. Speech Signal Process.*, 2011, pp. 4144–4147.

[34] M. A. Colominas, G. Schlotthauer, and M. E. Torres, "Improved complete ensemble EMD: A suitable tool for biomedical signal processing," *Biomed. Signal Process. Control*, vol. 14, no. 1, pp. 19–29, Nov. 2014.

[35] V. N. Vapnik, *The Nature of Stat. Learn. Theory*. New York, NY, USA:Springer, 2000.

[36] J. Suykens, J. De Brabanter, L. Lukas, and J. Vandewalle, "Weighted least squares support vector machines: Robustness and sparse approximation," *Neurocomputing*, vol. 48, no. 1–4, pp. 85–105, Oct. 2002.

[37] P. J. Rousseeuw and A. M. Leroy, *Robust Regression and Outlier Detection*. Hoboken, NJ, USA: Wiley, Oct. 1987.

[38] S. Hochreiter and J. Schmidhuber, "Long short-term memory," *Neural Comput.*, vol. 9, no. 8, pp. 1735–1780, Nov. 1997.

[39] B. Bole, C. S. Kulkarni, and M. Daigle, "Adaptation of an electrochemistry-based Li-ion battery model to account for deterioration observed under randomized use," in *Proc. Annu. Conf. Prognostics Health Manage. Soc.*, 2014, pp. 502–510.

Jianguo Wang was born in Jilin, China, in 1963. He received the B.S. and M.S. degrees in engineering from Tianjin University, Tianjin, China, in 1985 and 1988, respectively, and the Ph.D. degree from North China Electric Power University, Hebei, China, in 2001.

He is currently a Professor in automation engineering with Northeast Electric Power University, Jilin. His research interests include theory and technology of state intelligent diagnosis for power generating equipment, fouling monitoring of heat exchanger and its countermeasures, and fault monitoring and diagnosis of wind turbine, battery management system.

Shude Zhang (Student Member, IEEE) was born in Shandong, China, in 1995. He received the B.E. degree in automation in 2018 from Northeast Electric Power University, Jilin, China, where he is currently working toward the Ph.D. in control science and engineering.

His research interests include data-driven modeling, state estimation, and health management of lithium-ion batteries in electrical vehicles and energy storage systems.

Chenyu Li was born in Sichuan, China, in 1992. She received the B.E. degree in automation from the Hunan Institute of Technology, Hengyang, China, in 2015. She is currently working toward the M.E. degree in control engineering with Northeast Electric Power University, Jilin, China.

Her research interests include thermal effect and cooling design of lithium-ion batteries in electrical vehicles and energy storage systems.

Lifeng Wu received the B.S. degree in applied physics from the China University of Mining and Technology, Beijing, China, in 2002, the M.S. degree in detection technology and automation device from Northeast Electric Power University, Jilin, China, in 2005, and the Ph.D. degree in physical electronics from the Beijing University of Posts and Telecommunications, Beijing, in 2010.

From 2012 to 2013, he was a Visiting Scholar with Tsinghua University. From 2014 to 2015, he was a Postdoctoral with the University of Maryland, College Park, MD, USA. From 2017 to 2018, he was a Visiting Scholar with Peking University. He is currently a Professor with Capital Normal University, Beijing. His research interests include data-driven modeling, estimation and filtering, fault diagnosis, power electronics, and electrical vehicles.

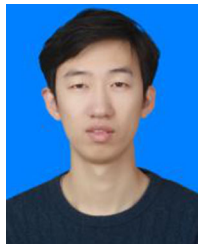

Yingzhou Wang was born in Shanxi, China, in 1987. He received the B.E. and M.E. degrees in control science and engineering from North China Electric Power University, Hebei, China, in 2011 and 2014, respectively, and the Ph.D. degree in power engineering from Northeast Electric Power University, Jilin, China, in 2021.

He is currently an Associate Professor with the School of Automation Engineering, Northeast Electric Power University. His research interests include state and life estimation, thermal effect, and fault diagnosis of lithium-ion batteries in electrical vehicles and energy storage.